journal

J. Am. Ceram. Soc., **88** [12] 3509–3512 (2005)
DOI: 10.1111/j.1551-2916.2005.00599.x

The ZrB_2 Volatility Diagram

William G. Fahrenholtz*,†

Materials Science and Engineering, University of Missouri-Rolla, Rolla, Missouri 65409

A volatility diagram was calculated for temperatures of 1000, 1800, and 2500 K to understand the oxidation of ZrB_2. Applying the diagram, it can be seen that exposure of ZrB_2 to air produces ZrO_2 (cr) and B_2O_3 (l) over the temperature range considered. The pressure of the predominant vapor species was predicted to increase from $\sim 10^{-6}$ Pa at 1000 K, to 344 Pa at 1800 K, and to $\sim 10^5$ Pa at 2500 K. Predictions were consistent with experimental observations that ZrB_2 exhibits passive oxidation below 1200 K, but undergoes active oxidation at higher temperatures due to B_2O_3 (l) evaporation.

I. Introduction

The borides, carbides, and nitrides of the early transition metals are considered ultra-high temperature ceramics (UHTCs) because of melting temperatures above 3000 K, high hardness, and resistance to chemical attack.[1,2] Among the UHTCs, zirconium diboride (ZrB_2) is a candidate for thermal protection systems and scramjet engine components for hypersonic flight vehicles as well as high temperature electrodes, molten metal containment systems, and incinerators.[3–6] Heating ZrB_2 in air produces a scale composed of ZrO_2 and B_2O_3.[7,8] Below 1200 K, liquid B_2O_3 forms a continuous layer that wets the ZrO_2 and the underlying ZrB_2. The B_2O_3 (l)[‡] layer acts as a barrier to oxygen diffusion resulting in passive oxidation of ZrB_2 and parabolic (diffusion-limited or $t^{1/2}$) oxidation kinetics.[9–11] At intermediate temperatures (1200–1700 K), the rates of formation and volatilization of B_2O_3 (l) are similar, resulting in para-linear kinetics because of competition between mass gain (ZrO_2 and B_2O_3 formation) and mass loss (B_2O_3 vaporization).[12,13] Above 1700 K, active oxidation with rapid linear kinetics has been attributed to loss of B_2O_3 (l) by evaporation, which leaves behind a porous, non-protective ZrO_2 (cr) layer.[7,14]

Interactions between gases and condensed phases can be interpreted with volatility diagrams.[15] Volatility diagrams plot the vapor pressure of the predominant gaseous species as a function of oxygen partial pressure and temperature. Gas–solid interactions have been studied for systems such as Mg–O, Al–O, Si–O, Si–C–O, Si–N–O, and Mg–O–C using volatility diagrams.[16–18] A recent study of UHTCs employed volatility diagrams for metals (e.g., Zr, Si, B) to evaluate the thermal stability of oxide scales.[19] However, to date, a true volatility diagram for ZrB_2 has not been reported. The diagram is needed to understand the oxidation of pure ZrB_2 as well as the oxidation of ZrB_2-based ceramics containing additives such as SiC, $MoSi_2$, or graphite.

The purpose of this paper is to describe the construction and interpretation of a volatility diagram for ZrB_2.

II. Calculations and Diagram Construction

Several thermodynamic databases were examined to identify relevant species containing Zr, B, and/or O, but only data from the NIST-JANAF tables were used to maximize consistency.[20] After eliminating ionized species, duplicate data, and condensed species that were not observed in oxidized specimens, 13 species of interest were identified (Table I). Based on oxidation studies reviewed in the introduction, the oxidation of ZrB_2 (cr) to ZrO_2 (cr) and B_2O_3 (l) by Eq. (1) was used to determine the equilibrium partial pressure of oxygen (pO_2) for oxidation of ZrB_2.

$$ZrB_2\ (cr) + \tfrac{5}{2}O_2\ (g) \rightarrow ZrO_2\ (cr) + B_2O_3\ (l) \tag{1}$$

Tabulated data were used to calculate the change in Gibbs' free energy (ΔG^0_{rxn}) for Reaction (1) and for reactions that produced volatile species from ZrB_2 (cr) or from ZrO_2 (cr) and B_2O_3 (l). The ΔG^0_{rxn} values were converted to equilibrium constant (K_{eq}) values using Eq. (2), and then to equilibrium partial pressures using expressions for the equilibrium constant for each reaction such as the one presented as Eq. (3) for Reaction (1). Unit activity was assumed for all condensed phases. The results are reported as partial pressures (e.g., no units, assuming an ambient pressure of 1.013×10^5 Pa or 1 atm). At 1800 K, the pO_2 calculated for the co-existence of ZrB_2 (cr), ZrO_2 (cr), and B_2O_3 (l) was 4.2×10^{-16} (vertical line in Fig. 1).

$$\Delta G^0_{rxn} = -RT\ \ln\ K_{eq} \tag{2}$$

where R is the ideal gas constant and T is the absolute temperature

$$K_{eq} = \frac{(a_{B_2O_3})(a_{ZrO_2})}{(a_{ZrB_2})(a_{O_2})^{5/2}} = \frac{1}{(pO_2)^{5/2}} \tag{3}$$

where a is the activity of the species involved in the reaction

Below the equilibrium pO_2 for Eq. (1), the gases are in equilibrium with ZrB_2 (cr). For example, B_2O_3 (g) can form by Eq. (4). Other gases that form by reaction of ZrB_2 are listed in Table II.

$$ZrB_2\ (cr) + \tfrac{5}{2}O_2\ (g) \rightarrow ZrO_2\ (cr) + B_2O_3\ (g) \tag{4}$$

As pO_2 increases, the amount of B_2O_3 (g) should increase since O_2 is a reactant. This relationship can be seen in the portion of

Table I. Zr, B, and O Species of Interest for Calculation of the Volatility Diagram

Zr species	Zr–O species	Zr–B species	B species	B–O species
Zr (g)	ZrO (g)	ZrB_2 (cr)	B (g)	B_2O_3 (g)
	ZrO_2 (cr)		B_2 (g)	B_2O_3 (l)
	ZrO_2 (g)			BO (g)
				BO_2 (g)
				B_2O (g)
				B_2O_2 (g)

A. Heuer—contributing editor

Manuscript No. 20394. Received April 8, 2005; approved May 15, 2005.
This material is based upon work supported by the National Science Foundation under Grant DMR 034680.
*Member, American Ceramic Society.
†Author to whom correspondence should be addressed. e-mail: billf@umr.edu
‡Note: The NIST-JANAF convention is used whereby physical state is indicated in parenthesis with (cr) for crystalline solids, (l) for liquids or amorphous solids, and (g) for gases.

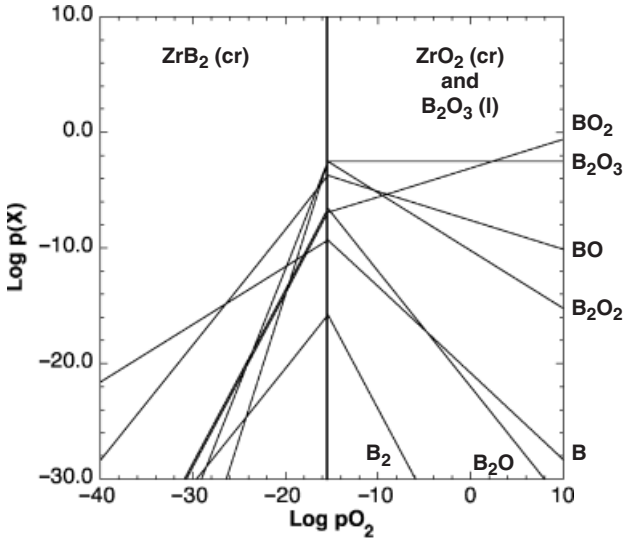

Fig. 1. Partial pressure of B species as a function of oxygen partial pressure at 1800 K.

Fig. 1 to the left of the ZrB_2/ZrO_2–B_2O_3 line. Above the equilibrium pO_2 for Eq. (1), the gases are in equilibrium with ZrO_2 (cr) and B_2O_3 (l). In this regime, B_2O_3 (g) forms by direct vaporization of B_2O_3 (l) according to Eq. (5).

$$B_2O_3\ (l) \rightarrow B_2O_3\ (g) \tag{5}$$

Because oxygen is neither consumed nor produced by Eq. (5), the partial pressure of B_2O_3 (g) does not vary with pO_2 (Fig. 1) in this regime. Other gases that form in this regime are listed in Table III. Pressures for all of the B-containing gases were determined in this manner and plotted in Fig. 1. The pressures of Zr-containing gases were calculated, but not plotted since they were much lower than those of B species. At the equilibrium pO_2 for Eq. (1), the partial pressure of B_2O_3 (g) above ZrB_2 (cr) must be the same as it is above ZrO_2 (cr)–B_2O_3 (l) since the gas is in equilibrium with all of the condensed phases simultaneously. Pressures for all of the gases met this criterion for consistency, which can be seen in Fig. 1 for B-containing gases.

The vapor pressures of all of the gases were calculated to compile a volatility diagram at 1800 K (Fig. 2(a)). The system undergoes four major vapor transitions at 1800 K: (1) from B (g) to BO (g) at a pO_2 of $\sim 2 \times 10^{-27}$; (2) from BO (g) to B_2O_2 (g) at a pO_2 of $\sim 3 \times 10^{-17}$; (3) from B_2O_2 (g) to B_2O_3 (g) at a pO_2 of $\sim 3 \times 10^{-16}$; and (4) from B_2O_3 (g) to BO_2 (g) at a pO_2 of $\sim 8 \times 10^{1}$. Vapor pressure calculations were also completed at 1000 and 2500 K to show how the diagram changed with temperature (Fig. 2(b)). Interestingly, the transition from stability of B_2O_2 (g) to B_2O_3 (g) falls near the equilibrium pO_2 for Eq. (1) ($\sim 4 \times 10^{-16}$) at 1800 K and also at 2500 K so that the vapor transition is obscured by the transition in stable condensed phases.

III. Discussion

The volatility diagram was used to interpret experimental observations of ZrB_2 oxidation in air. At 1000 K, the predominant species above B_2O_3 (l) and ZrO_2 (cr) was BO_2 (g) with a partial pressure of $\sim 10^{-11}$ ($\sim 10^{-6}$ Pa). The next highest vapor pressure was $\sim 10^{-12}$ ($\sim 10^{-7}$ Pa) for B_2O_3 (g). The calculated pressures of the other species were all dramatically lower (Table IV). The vaporization rate for B_2O_3 (l) in air is expected to be low at 1000 K based on the partial pressures of the various gases, none of which exceeds $\sim 10^{-11}$.

Above $\sim$1650 K, rapid, linear (active) oxidation kinetics have been attributed to a significant increase in the rate of B_2O_3 (l) evaporation.[7] Examination of ZrB_2 oxidized at 1773 K by scanning electron microscopy (Fig. 3) and X-ray diffraction (not shown) revealed that the oxide layer was made up almost exclusively of porous ZrO_2 (cr), which does not provide passive oxidation protection. From the volatility calculations, the predominant vapor species at 1800 K in air was B_2O_3 (g) with a pressure of $\sim 10^{-2}$ (344 Pa). Two other species had vapor pressures predicted to be greater than 10^{-10} ($\sim 10^{-5}$ Pa) at 1800 K in air, BO_2 (g) at $\sim 10^{-3}$ (86 Pa), and BO (g) at $\sim 10^{-8}$ ($\sim 10^{-3}$ Pa). Based on the nine order of magnitude increase in the pressure of the dominant species compared to 1000 K, the rate of B_2O_3 (l) vaporization would be expected to be significantly higher at 1800 K, which is consistent with B_2O_3 evaporation from the surface of ZrB_2 that is oxidized in air at 1650 K or above. Active oxidation of ZrB_2 is also expected at higher temperatures, unless the ZrO_2 scale becomes protective. Oxidation of ZrB_2-SiC above 2000 K in arc jet testing suggests that ZrO_2 may become protective at these temperatures by sintering into a coherent scale.[21]

Table II. Volatilization Reactions Involving ZrB_2 (cr) as the Primary Condensed Phase

Reactions producing volatile B species	Reactions producing volatile Zr species
$ZrB_2\ (cr)+3O_2\ (g) \rightarrow ZrO_2\ (cr)+2BO_2\ (g)$	$ZrB_2\ (cr)+\frac{5}{2}O_2\ (g) \rightarrow ZrO_2\ (g)+B_2O_3\ (l)$
$ZrB_2\ (cr)+\frac{5}{2}O_2\ (g) \rightarrow ZrO_2\ (cr)+B_2O_3\ (g)$	$ZrB_2\ (cr)+2O_2\ (g) \rightarrow ZrO\ (g)+B_2O_3\ (l)$
$ZrB_2\ (cr)+2O_2\ (g) \rightarrow ZrO_2\ (cr)+B_2O_2\ (g)$	$ZrB_2(cr)+\frac{3}{2}O_2(g) \rightarrow Zr(g)+B_2O_3(l)$
$ZrB_2\ (cr)+2O_2\ (g) \rightarrow ZrO_2\ (cr)+2BO\ (g)$	
$ZrB_2\ (cr)+\frac{3}{2}O_2\ (g) \rightarrow ZrO_2\ (cr)+B_2O\ (g)$	
$ZrB_2\ (cr)+O_2\ (g) \rightarrow ZrO_2\ (cr)+B_2\ (g)$	
$ZrB_2\ (cr)+O_2\ (g) \rightarrow ZrO_2\ (cr)+2B\ (g)$	

Table III. Volatilization Reactions Involving ZrO_2 (cr) and B_2O_3 (l) as the Primary Condensed Phases

Reactions producing volatile B species	Reactions producing volatile Zr species
$B_2O_3\ (l) \rightarrow B_2O_3\ (g)$	$ZrO_2\ (cr) \rightarrow ZrO_2\ (g)$
$B_2O_3\ (l)+\frac{1}{2}O_2\ (g) \rightarrow 2BO_2(g)$	$ZrO_2\ (cr) \rightarrow ZrO(g)+\frac{1}{2}O_2\ (g)$
$B_2O_3(l) \rightarrow B_2O_2\ (g)+\frac{1}{2}O_2\ (g)$	$ZrO_2\ (cr) \rightarrow Zr\ (g)+O_2\ (g)$
$B_2O_3\ (l) \rightarrow 2BO\ (g)+\frac{1}{2}O_2\ (g)$	
$B_2O_3\ (l) \rightarrow B_2O\ (g)+O_2\ (g)$	
$B_2O_3\ (l) \rightarrow B_2\ (g)+\frac{3}{2}O_2\ (g)$	
$B_2O_3\ (l) \rightarrow 2B\ (g)+\frac{3}{2}O_2\ (g)$	

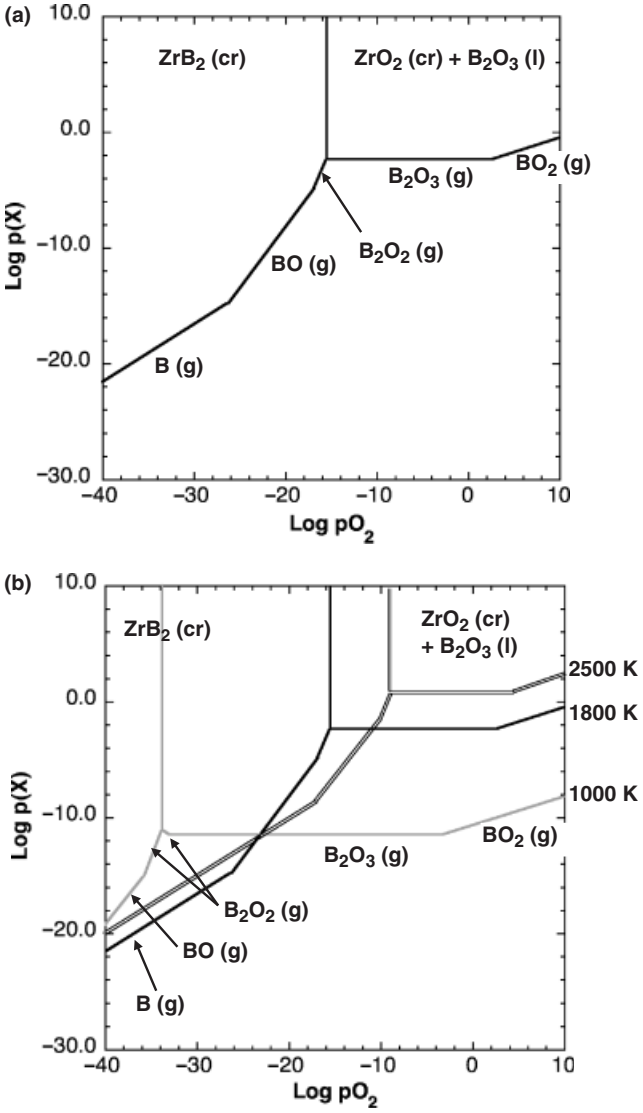

Fig. 2. The full volatility diagram for zirconium diboride (ZrB_2) at (a) 1800 K and (b) at 1000, 1800, and 2500 K.

IV. Summary

A volatility diagram was calculated for ZrB_2. The diagram defines equilibrium pO_2 values for the transition from ZrB_2 (cr) to ZrO_2 (cr) and B_2O_3 (l) as a function of temperature. In addition, the diagram shows the vapor pressure of the predominant vapor species as a function of temperature and pO_2. At 1000 K, exposure to air resulted in passive oxidation due to the formation of a surface layer of B_2O_3 (l). The partial pressure of the predominant species, BO_2 (g), was predicted to be 10^{-11} (10^{-6} Pa) at 1000 K in air, consistent with the observation of passive oxidation. Increasing the temperature to 1800 K in air increased the partial pressure of the predominant species, B_2O_3 (g), to $\sim 10^{-2}$ (344 Pa). The substantial increase in vapor pressure was consistent with the observed transition from passive to active oxidation kinetics between these temperatures.

Table IV. Partial Pressures of all Vapor Species for Oxidation in Air ($pO_2 = 0.2$) at 1000, 1800, and 2500 K

	Partial pressure		
Species	1000 K	1800 K	2500 K
BO_2 (g)	1×10^{-11}	6×10^{-4}	2×10^{-1}
B_2O_3 (g)	3×10^{-12}	3×10^{-3}	3.3
B_2O_2 (g)	2×10^{-28}	1×10^{-10}	2×10^{-4}
BO (g)	3×10^{-22}	4×10^{-8}	3×10^{-3}
B_2O (g)	1×10^{-52}	5×10^{-22}	1×10^{-11}
B_2 (g)	3×10^{-86}	1×10^{-38}	4×10^{-22}
B (g)	3×10^{-48}	5×10^{-21}	1×10^{-11}
ZrO_2 (g)	8×10^{-32}	2×10^{-13}	4×10^{-7}
ZrO (g)	1×10^{-47}	2×10^{-20}	5×10^{-11}
Zr (g)	7×10^{-72}	2×10^{-33}	7×10^{-19}

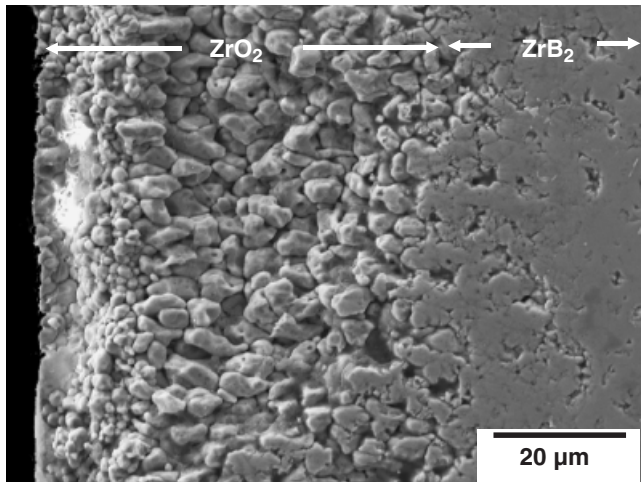

Fig. 3. A zirconium diboride (ZrB_2) ceramic oxidized at 1773 K in air for 30 min showing a surface layer of porous ZrO_2.

Acknowledgments

The author thanks Drs. Mark Opeka and Inna Talmy of the Naval Surface Warfare Center-Carderock Division and Professor Jeff Smith of UMR for many educational discussions. The SEM image was provided by UMR graduate student Adam Chamberlain.

References

[1]R. Telle, L. W. Sigl, and K. Takagi, "Boride-Based Hard Materials"; pp. 802–945 in *Handbook of Ceramic Hard Materials*, Edited by R. Riedel. Wiley-VCH, Weinheim, 2000.

[2]R. A. Cutler, "Engineering Properties of Borides"; pp. 787–803 in *Ceramics and Glass: Engineered Materials Handbook*, Vol. 4. Edited by S. J. Schneider Jr.. ASM International, Materials Park, OH, 1991.

[3]T. A. Jackson, D. R. Eklund, and A. J. Fink, "High Speed Propulsion: Performance Advantage of Advanced Materials," *J. Mater. Sci.*, **39** [19] 5905–13 (2004).

[4]D. M. Van Wie, D. G. Drewry Jr., D. E. King, and C. M. Hudson, "The Hypersonic Environment: Required Operating Conditions and Design Challenges," *J. Mater. Sci.*, **39** [19] 5915–24 (2004).

[5]K. Kuwabara, S. Sakamoto, O. Kida, T. Ishino, T. Kodama, H. Nakajima, T. Ito, and Y. Hirakawa "Corrosion Resistance and Electrical Resistivity of ZrB_2 Monolithic Refractories"; pp. 302–5 in *Proceedings of UNITECR 2003, the 8th Biennial Worldwide Conference on Refractories*, Osaka, Japan, October 19–22, 2003, Edited by K. Asano. The Technical Association of Refractories, Tokyo, 2003.

[6]S. Kinoshita, Y. Miyagishi, and Y. Ono "Application of Zirconium Diboride Materials to Waste Melting Furnace"; pp. 205–8 in *Proceedings of UNITECR 2003, the 8th Biennial Worldwide Conference on Refractories*, Osaka, Japan, October 19–22, 2003, Edited by K. Asano. The Technical Association of Refractories, Tokyo, 2003.

[7]W. C. Tripp and H. C. Graham, "Thermogravimetric Study of the Oxidation of ZrB_2 in the Temperature Range of 800° to 1500°C," *J. Electrochem. Soc.*, **118** [7] 1195–9 (1971).

[8]L. Kaufman, E. V. Clougherty, and J. B. Berkowitz-Mattuck, "Oxidation Characteristics of Hafnium and Zirconium Diboride," *Trans. Metall. Soc. AIME*, **239** [4] 458–66 (1967).

[9]J. B. Berkowitz-Mattuck, "High Temperature Oxidation: III. Zirconium and Hafnium Diborides," *J. Electrochem. Soc.*, **113** [9] 908–14 (1966).

[10]R. J. Irving and I. G. Worsley, "The Oxidation of Titanium Diboride and Zirconium Diboride at High Temperatures," *J. Less-Common Metals*, **16**, 103–12 (1968).

[11]J. R. Shappirio, J. J. Finnegan, R. A. Lux, and D. C. Fox, "Resistivity, Oxidation Kinetics, and Diffusion Barrier Properties of Thin Film ZrB_2," *Thin Solid Films*, **119** [1] 23–30 (1984).

[12]H. C. Graham, H. H. Davis, I. V. Kvernes, and W. C. Tripp, "Microstructural Features of Oxide Scales Formed on Zirconium Diboride Materials"; pp. 35–48 in

Materials Science Research, Volume 5: Ceramics in Severe Environments, Edited by W. W. Kriegel, and H. Palmour III. Plenum Press, New York, 1971.

[13]I. G. Talmy, J. A. Zaykoski, and M. M. Opeka, "Properties of Ceramics in the ZrB_2/ZrC/SiC System Prepared by Reactive Processing," *Ceram. Eng. Sci. Proc.*, **19** [3] 105–112 (1998).

[14]A. K. Kuriakose and J. L. Margrave, "The Oxidation Kinetics of Zirconium Diboride and Zirconium Carbide at High Temperatures," *J. Electrochem. Soc.*, **111** [7] 827–31 (1964).

[15]V. L. K. Lou, T. E. Mitchell, and A. H. Heuer, "REVIEW—Graphical Displays of the Thermodynamics of High-Temperature Gas–Solid Reactions and Their Application to Oxidation of Metals and Evaporation of Oxides," *J. Am. Ceram. Soc.*, **68** [2] 49–58 (1985).

[16]A. H. Heuer and V. L. K. Lou, "Volatility Diagrams for Silica, Silicon Nitride, and Silicon Carbide and Their Application to High Temperature Decomposition and Oxidation," *J. Am. Ceram. Soc.*, **73** [10] 2785–3128 (1990).

[17]J. D. Smith "Reaction Chemistry and Thermochemistry of Magnesia–Graphite Systems Containing Anti-Oxidants"; Ph.D. Thesis, University of Missouri-Rolla, 1993.

[18]B. Schneider, A. Guette, R. Naslain, M. Cataldi, and A. Costecalde, "A Theoretical and Experimental Approach to the Active-to-Passive Transition in the Oxidation of Silicon Carbide," *J. Mater. Sci.*, **33** [2] 535–47 (1998).

[19]M. M. Opeka, I. G. Talmy, and J. A. Zaykoski, "Oxidation-Based Materials Selection for 2000°C+ Hypersonic Aerosurfaces: Theoretical Considerations and Historical Experience," *J. Mater. Sci.*, **39** [19] 5887–904 (2004).

[20]M. W. Jr. Chase, *NIST-JANAF Thermochemical Tables*, 4th edition, American Institute of Physics, Woodbury, NY, 1998.

[21]A. L. Chamberlain, W. G. Fahrenholtz, G. E. Hilmas, and D. T. Ellerby. "Oxidation of ZrB_2–SiC Ceramics Under Atmospheric and Reentry Conditions," *Refractory Appl. Trans.*, **1** [2] 2–8 (2005). □